CrossMark

Effect of Post-Deposition Annealing on RF-Sputtered Catalyst-Free Grown ZnO Nanostructures

AMIT SRIVASTAVA[1] and NARESH KUMAR [1,2,3]

1.—Department of Physics, Motilal Nehru National Institute of Technology Allahabad, Allahabad 211004, India. 2.—e-mail: nsisodia@mnnit.ac.in. 3.—e-mail: n_sisodia@yahoo.com

Catalyst-free zinc oxide (ZnO) nano-structures were synthesized on silicon (100) substrate by radio frequency sputtering. The as-deposited films were post-annealed at 200°C, 400°C, 600°C, and 800°C. The effects of annealing temperature on the structural, morphological and optical properties of these nanostructures were investigated using x-ray diffraction (XRD), atomic force microscopy (AFM) and spectroscopic ellipsometry. XRD showed c-axis-oriented growth with the increase in crystallinity at the higher annealing temperature of these ZnO nanostructures. The crystallite size calculated using Scherrer's formula in the XRD data was found to increase with the annealing temperature. AFM images confirmed the growth of grains at higher annealing temperatures. Optical band gaps of these ZnO nanostructures were calculated using reflectance spectra in the ultraviolet–visible region and found to decrease from 3.19 eV to 3.09 eV as the annealing temperature increased from 200°C to 800°C. The decrease in band gap may be attributed to the decrease in oxygen vacancies at higher annealing temperatures and may be useful for different applications.

Key words: RF sputtering, ZnO, nanostructures, XRD, AFM

INTRODUCTION

Zinc oxide (ZnO) is a wide band gap (3.37 eV) semiconductor of the II–IV group with large exciton binding energy (60 MeV).[1] It is currently subject to numerous studies because of its exceptional properties such as abundance in nature and lack of toxicity, high transparency in the visible region, stability and low cost. These properties allow it to be a material model especially in its extremely various applications such as solar cells, various optoelectronic devices, gas sensors, Schottky diodes, ultraviolet light-emitting diodes (LEDs), etc.[2,3] In recent years, ZnO nanostructures have also been reported to have potential applications for optical emission, catalysis, sensing, actuation and drug delivery. The increase in surface area and quantum confinement effects has made ZnO nanostructures quite different from their bulk counterparts.[4] Exhaustive research has been focused on synthesizing the different ZnO

nanostructures and correlating their morphology with their structural, optical and surface morphological properties. ZnO thin films have been prepared by various techniques such as thermal evaporation,[5] pulsed laser deposition (PLD),[6] molecular beam epitaxy,[7] magnetron sputtering,[8] sol–gel,[9] chemical vapor deposition[10] and spray pyrolysis.[11] Among these, the radio frequency (RF) sputtering deposition technique is one of the known techniques with several advantages such as better film growth control, repeatability, low temperature deposition, large-scale stability and uniform film properties.[8,12] During the synthesis of ZnO nanostructures in sputtering, the growth conditions such as nature of the substrate, deposition temperature, background gas pressure and RF power have great influence on the growth quality of the ZnO nanostructure and influences optical and structural properties to quite an extent. It has also been reported that annealing of nanostructures after the deposition helps in improving their structural, morphological and optical properties. Asmar et al.[13]

reported the effect of annealing on the electrical and optical properties of electron beam-evaporated ZnO thin films grown on a silicon substrate. It has been observed that annealing treatment decreases the full width at half maximum (FWHM) in XRD data of these films, thus refining the crystallinity of the films. However, no significant change in surface roughness has been observed after annealing. Joydip et al.[14] studied the influence of annealing temperature on the structural, topographical and optical properties of sol–gel-derived ZnO thin films. The study revealed that the films have a preferred orientation along the (002) plane and crystallinity along with grain size augmented with annealing temperature. Additionally, annealing roughed the surface of the film. Similar results were also reported by Yidong et al.,[15] in which ZnO nanostructures were prepared by the sol–gel method and post-annealed up to 600°C in air for 1 h. Rusop et al.[16] reported the effect of post-growth annealing of pulsed laser-deposited ZnO thin films grown on quartz and silicon substrates under enhanced oxygen pressure. The intensity of XRD peaks corresponding to the (002) reflection was observed to be increased with an increase in annealing temperature. Also, the FWHM value decreased for higher annealing temperatures resulting in an increase in crystallite size. Similarly, Zhu et al.[17] studied the low-temperature annealing (150–450°C) effect on the structural and optical properties of PLD-grown ZnO films on the glass substrate and found improvements in grain size and stoichiometric ratio with annealing temperature contributing to the enhancement in UV emissions. Fang et al.[18] and Daniel et al.[19] have studied the influence of post-annealing treatment on the structural properties of ZnO films grown by RF sputtering, and observed an improvement in crystallinity, oriented growth along the (002) plane, an increase in surface roughness and a ecrease in the direct band gap with the increase in annealing temperature.

In the present study, we report on the growth of (00l)-oriented ZnO nanostructures without using any catalyst on a Si (100) substrate by RF sputtering. The effect of post-deposition annealing on the structural, surface morphology and optical properties of ZnO nanostructures have been carried out and are presented.

EXPERIMENTAL

Zinc oxide (99.99%; Sigma-Aldrich, USA) was used for preparing the target required for the growth of ZnO nanostructures on a single crystal Si (100) substrate using RF sputtering. The target was prepared by applying a pressure of 5 t/sq. in. on a pellet-making die for 5 min. The prepared target was sintered at a temperature of 1000°C and sputtered in the reactive gas mixture (Ar: 5 sccm + O_2: 40 sccm) at a power of 300 W in 5×10^{-6} mbar of vacuum for the synthesis of ZnO

nanostructures at ambient temperature. After the deposition, samples were annealed in a tube furnace at 200°C, 400°C, 600°C, and 800°C for 1 h in air. Prior to the deposition, Si substrates were cleaned with the RCA process (Radio Corporation of America) in the sequence of RCA1 and RCA2. The optimized deposition conditions used for the deposition of ZnO nanostructures on Si substrate are described in Table I.

The crystal structure of the ZnO nanostructure was studied by using x-ray diffraction (XRD) [Model: Rigaku Smart lab 3 kW, Japan with CuKα radiation (λ = 1.540 Å)]. Surface morphology of the ZnO nanostructures was also investigated using atomic force microscopy (AFM) (Agilent 5500). Optical properties and thickness of the films were calculated using a spectroscopic ellipsometer (VASE; J.A. Wollam).

RESULTS AND DISCUSSION

The XRD patterns for ZnO nanostructures annealed in a temperature range of 200–800°C are represented in Fig. 1a (the XRD intensity is plotted on a log scale). It can be seen from the XRD data that the nanostructure deposited at ambient temperature and annealed at 200°C shows one clear peak at 34.5° and a hump near 72°. The peak and hump were indexed with as (002) and (004) reflections of ZnO using standard ICDD data file 01-080-300. When the nanostructure was annealed at the higher temperatures of 400°C, 600°C, and 800°C, the reflection intensity of the (002) peak gradually increased and the hump corresponding to the (004) refection converted into a clear peak. This suggests c-axis growth of ZnO on the Si substrate and that the crystallinity of the samples increases with the increase in annealing temperature. The gradual increase in the intensity of the (002) orientation may be due to the high annealing temperature which provides enough energy to enhance the mobility which could decrease the defects in the ZnO films.[18] In a similar study, Kim et al.[20] deposited ZnO nanostructures by RF sputtering and the effect of annealing temperature on crystal structure was investigated. It was observed that the ZnO nanostructure grows along the preferred c-axis and the crystallinity of the film increased with the increase in annealing temperature.

The FWHM of the (002) peak was used to calculate the crystallite size of the ZnO samples annealed at different temperatures using Scherer's formula, shown by Eq. 1.[24]

$$D = \frac{0.9\lambda}{\beta\cos\theta} \qquad (1)$$

where λ, β, θ are the x-ray wavelength, FWHM and Bragg's diffraction angle of the (002) diffraction peak, respectively. The calculated value of FWHM and crystallite size has been plotted against

Table I. Deposition conditions used for ZnO nanostructure on Si substrate

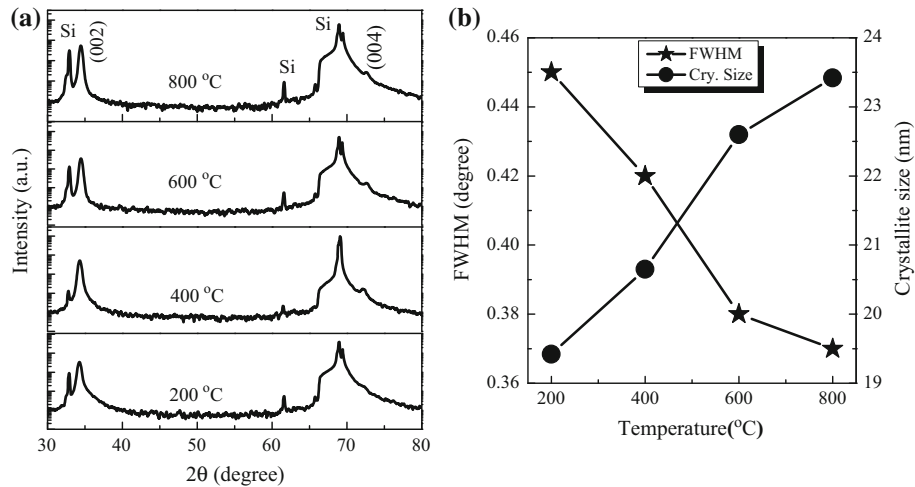| Conditions for the ZnO nanostructure	
Target substrate distance	10.0 cm
Base vacuum	1.00×10^{-6} m-bar
Deposition pressure	5×10^{-6} m-bar
Ar:O_2 pressure (sccm)	5:40
Deposition time	1 h
RF power (W)	300 W

Fig. 1. (a) XRD pattern of ZnO nanostructures annealed at 200°C, 400°C, 600°C, and 800°C. (b) Variation of crystallite size and FWHM with annealing temperature.

annealing temperature and is shown in Fig. 1b. As seen from the figure, the crystallite size increased gradually from 19 nm to 23 nm when the samples were annealed from 200°C to 800°C. Diffusion of atoms absorption on the substrate thereby accelerating the migration of atoms to the favorable energy positions is preferential by increasing the annealing temperature. This results into the enhancement of the crystallinity and c-axis orientation of ZnO nanostructures, which has been indicated by the increased intensity of the (002) peak and decrease of the FWHM value for the ZnO nanostructures.[16] In addition, FWHM/crystallite size does not follow linear variation with temperature (Fig. 1b). The non-linear change in crystalline size with the annealing temperature may be due to the fact that at higher temperatures crystallites gain higher energy and small crystallites segregate into larger grains. Yang et al.[21] and Sengupta et al.[14] also observed that the grain size of ZnO films increases with increasing annealing temperature.

The surface morphology of the ZnO nanostructures was characterized by AFM and the topographical 2-dimensional AFM images of ZnO nanostructures annealed at the temperatures of 200°C, 400°C, 600°C, and 800°C are shown in Fig. 2.

It can be seen from the morphographs that the surface of the films shows granular growth with nanocrystalline morphologies. The grain size distribution was determined using histogram plots. By fitting the frequency plot, the average grain size of ZnO at different annealing temperatures was determined. The average grain size and RMS roughness for the sample annealed at 200°C were measured as 37 nm and 1.6 nm, respectively. It can be seen from Fig. 3 that, with increasing annealing temperature, both average grain size and RMS roughness were increased. It should be mentioned that the grain size calculated using AFM is larger than the crystallite size estimated using XRD data which may be due to the accumulation of smaller grains which form bigger clusters on the surface of the films. Annealing ZnO nanostructures at elevated temperatures, the defects at the grain boundaries (oxygen and/or oxygen defects) favor the merging process by stimulating the coalescence of more grains. Fang et al.[18] also observed that the increase in average grain size and RMS roughness may also be attributed to the fact that, at a higher temperature, the atoms have sufficient diffuse activation energy which will help to occupy the correct site in the crystal lattice and result in larger grains with

lower surface energy. In a similar study by Lee
et al.,[28] it has been observed that roughness and
grain size increase with the increase in annealing
temperature which may be due to the integration of
the grains. Daniel et al.[19] and Karamdel et al.[23] also
reported that the RMS roughness of ZnO nanostructures increased with an increasing annealing
temperature.

The optical band gaps of the annealed ZnO
nanostructures were studied with the help of
reflectance spectra in the UV–visible region. Figure 4a shows a graph between $h\nu$ (abscissa) and the
square of $ln\ [(R_{max} - R_{min})/(R - R_{min})]$. The calculated value of the optical band gap has been plotted
against annealing temperature and is shown in
Fig. 4b. It can be observed from the figure that the
optical band gaps of samples gradually decrease
from 3.19 eV to 3.09 eV when the annealing temperature increased from 200°C to 800°C. In the ZnO
nanostructures, the surface defects play a significant role in the control of the band gap. The defect
states like Zn interstitials (Zn_i), Zn vacancy (V_{Zn}),
oxygen vacancies (V_O), etc. can be accommodated
easily in ZnO as it has a relatively open structure
with a hexagonal close-packed lattice. In this lattice,
Zn atoms occupy half of the tetrahedral sites, while
the octahedral sites remain vacant. In such vacant
sites, there is a good possibility for accommodating
such defects. The stoichiometric excess of Zn may
also be possible when annealed at a higher temperature as oxygen evaporates prior to zinc due to a
higher vapor pressure. Ionization energies corresponding to such defects may vary from ~0.05 eV to
2.8 eV.[29] These defects fade away at a higher
annealing temperature and may affect the band

gap of the ZnO nanostructures.[29] The decrease in
optical band gap with increasing temperature has
also been reported by Mandal et al.[25] in ZnO
nanostructures and attributed to the compressive
strain in the deposited ZnO nanostructure. After
increasing the deposition temperature, the band
gap value decreases due to the relaxation of the
built-in strain. It has been observed by Wahab
et al.[26] that, when the annealing temperature
increases, there is a decrease in optical band gap
with a slight blue shift in ZnO nanostructures
which may be because, with increasing annealing
temperature, the stoichiometry of the ZnO nanostructures were improved, i.e. the defect number
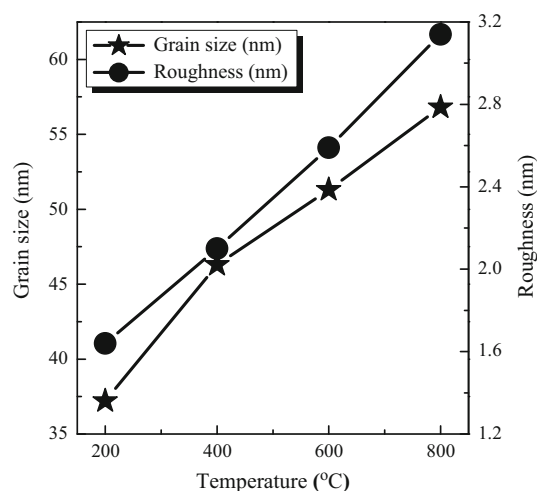

Fig. 3. Variation of grain size calculated using AFM images and
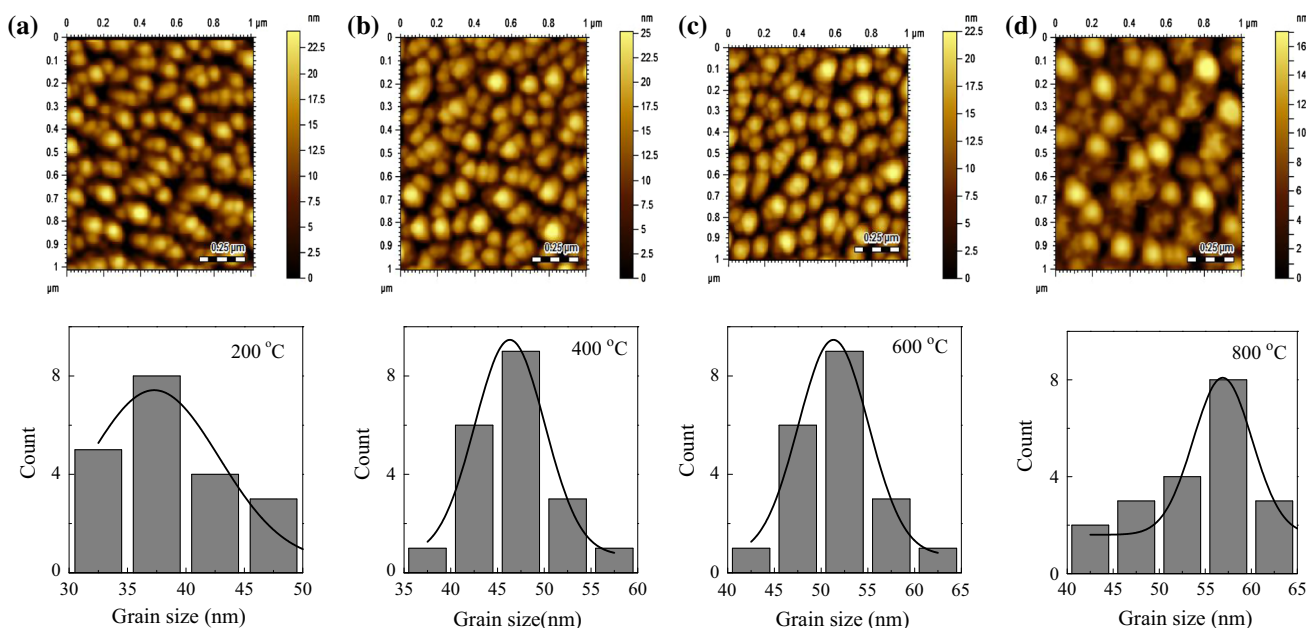roughness with increasing annealing temperature.

Fig. 2. Topological 2-dimensional AFM images of ZnO nanostructures annealed at (a) 200°C (b) 400°C (c) 600°C (d) 800°C (up to down).
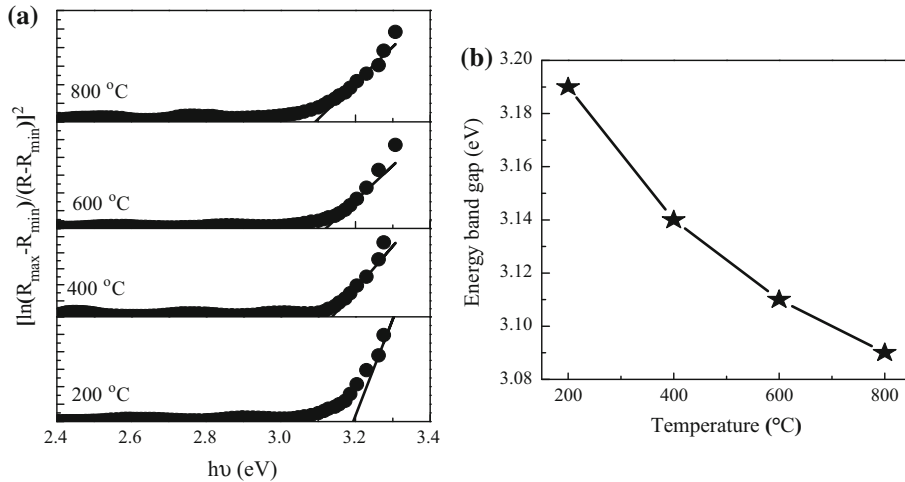Histogram plots are shown adjacent to the images. [Color online].

Fig. 4. (a) $[\ln\{(R_{max} - R_{min})/(R - R_{min})\}]^2$ versus hυ plot for ZnO nanostructures annealed in the temperature range of 200–800°C. (b) Variation of annealing temperature with optical band gap.

decreases. Kang et al.[27] explained that the change in optical band gap is related to the structural property of ZnO film. Since ZnO thin film has a tensile built-in strain, the tensile strain in ZnO could be relaxed by providing sufficient thermal energy. If the tensile strain is relaxed, the band gap energy is decreased. Danial et al.[19] also explained that, due to thermal expansion, the periodic potential experienced by the electrons (and hence the band gap structure and energy gap) varied with temperature. The effect of lattice vibrations on the band structure and energy gap also varies with the temperature. These two effects may be responsible for the decrease in band gap with the increase in annealing temperature. It could also be noticed that, when the ZnO nanostructures were annealed in air, the number of oxygen vacancies decreased and the carrier concentration in the conduction band also decreased.[22] Hence, the Fermi level moved down and the band gap decreased.

CONCLUSION

Catalyst-free (001)-oriented zinc oxide (ZnO) nanostructures were deposited by RF sputtering onto a Si (100) substrate at room temperature. The growth quality has been found to increase with the post-deposition annealing of ZnO nanostructures. Moreover, the annealing treatment improves the morphology of the ZnO nanostructures which can be seen from AFM images. It was also observed from AFM data that the grain size and surface roughness increases with increases in the annealing temperature which may be due to grain growth. The band gap was calculated using reflectance spectra in the UV–vis region. The optical band gap was decreased from 3.19 eV to 3.09 eV with the increase in annealing temperature/grain size. The decrease in band gap for the film annealed at a higher temperature may be attributed to the decrease in oxygen

vacancies and may be useful for different applications.

REFERENCES

1. S.K. Arya, S. Saha, J.E. Ramirez-Vick, V. Gupta, S. Bhansali, and S.P. Singh, *Rev. Anal. Chim. Acta* 737, 1 (2012).
2. S.E. Volkan, P. Suat, S.K. Adan, A. Tuna, E. Saliha, O. Soner, E. Naci, and M.B. Zafer, *Appl. Surf. Sci.* 318, 2 (2014).
3. X. Duan, Y. Huang, Y. Cui, J. Wang, and C.M. Lieber, *Nature* 409, 66 (2001).
4. J. Elias, J. Michler, L. Philippe, M.-Y. Lin, C. Couteau, G. Lérondel, and C. Lévy-Clément, *J. Electron. Mater.* 40, 728 (2011).
5. J.F. Ghislain, F. Yamin, S. Moussa, and H. Xintang, *Mater. Sci. Semicond. Process.* 16, 652 (2013).
6. K.J. Raied, A.H. Mohammed, and A.A. Kadhim, *Mater. Lett.* 132, 31 (2014).
7. T.C. Zhang, Z.X. Mei, A.Y. Kuznetsov, and X.L. Du, *J. Cryst. Growth* 325, 93 (2011).
8. A. Ismail and M.J. Abdullah, *J. King Saud Univ. Sci.* 25, 209 (2013).
9. A.J. Hashim, M.S. Jaafar, J.G. Alaa, and N.M. Ahmed, *Opt. Int. J. Light Electron. Opt.* 124, 491 (2013).
10. J.C. Hsiao, H.C. Chen, H.J. Yang, C.L. Wu, C.F. Huang, C.C. Lin, P. Yu, and J.C. Hwang, *J. Taiwan Inst. Chem. Eng.* 44, 758 (2013).
11. A. Zaier, F. OumElaz, F. Lakfif, A. Kabir, S. Boudjadar, and M.S. Aida, *Mater. Sci. Semicond. Process.* 12, 207 (2009).
12. G.C. Yi, C. Wang, and W. Park, *Semicond. Sci. Technol.* 20, S22 (2005).
13. R.A. Asmar, G. Ferblantier, F. Mailly, P.G. Borrut, and A. Foucaran, *Thin Solid Films* 473, 49 (2005).
14. J. Sengupta, R.K. Sahoo, K.K. Bardhan, and C.D. Mukherjee, *Mater. Lett.* 65, 2572 (2011).
15. Y. Zhang, W. Fa, F. Yang, Z. Zheng, and P. Zhang, *Ionics* 16, 815 (2010).

16. M. Rusop, K. Uma, T. Soga, and T. Jimbo, *Mater. Sci. Eng. B* 127, 150 (2006).
17. B.L. Zhu, X.Z. Zhao, F.H. Su, G.H. Li, X.G. Wu, J. Wu, and R. Wu, *Vacuum* 84, 1280 (2010).
18. Z.B. Fang, Z.J. Yan, Y.S. Tan, X.Q. Liu, and Y.Y. Wang, *Appl. Surf. Sci.* 241, 303 (2005).
19. G.P. Daniel, V.B. Justinvictor, P.B. Nair, K. Joy, P. Koshy, and P.V. Thomas, *Phys. B* 405, 1782 (2010).
20. K.S. Kim, H.W. Kim, and N.H. Kim, *Phys. B* 334, 343 (2003).
21. J. Yang, M. Gao, Y. Zhang, L. Yang, J. Lang, D. Wang, H. Liu, Y. Liu, Y. Wang, and H. Fan, *Superlattices Microstruct.* 44, 137 (2008).
22. J.F. Guojia, L. Dejie, and L.Y. Bao, *Thin Solid Films* 418, 156 (2002).
23. J. Karamdel, C.F. Dee, and B.Y. Majlis, *Sains Malays.* 40, 209 (2011).
24. L.V. Azaroff, *Elements of X-ray Crystallography* (New York: McGraw Hill, 1968).
25. S. Mandal, R.K. Singha, A. Dhar, and S.K. Ray, *Mater. Res. Bull.* 43, 244 (2008).
26. H.A. Wahab, A.A. Salama, A.A. El-Saeid, O. Nur, M. Willander, and I.K. Battisha, *Results Phys.* 3, 46 (2013).
27. H.S. Kang, J.S. Kang, J.W. Kim, and S.Y. Lee, *J. Appl. Phys.* 95, 1246 (2004).
28. C. Lee, J.H. Kim, and S.K. Shin, *J. Korean Phys. Soc.* 53, 3021 (2008).
29. L.S. Mende and J.L. MacManus-Driscoll, *Mater. Today* 10, 40 (2007).